Earth's Alfvén wings driven by the April 2023 Coronal Mass Ejection

Li-Jen Chen[1], Daniel Gershman[1], Brandon Burkholder[1], Yuxi Chen[2], Menelaos Sarantos[1], Lan Jian[1], James Drake[3], Chuanfei Dong[2], Harsha Gurram[1,3], Jason Shuster[4], Daniel Graham[5], Olivier Le Contel[6], Steven Schwartz[7], Hadi Madanian[8], Craig Pollock[9], Haoming Liang[1,3], Matthew Argall[4], Richard Denton[10], Rachel Rice[1,3], Jason Beedle[4], Kevin Genestreti[4,11], Akhtar Ardakani[4], Adam Stanier[12], Ari Le[12], Jonathan Ng[1,3], Naoki Bessho[1,3], Megha Pandya[1], Frederick Wilder[13], Christine Gabrieles[14], Ian Cohen[15], Hanying Wei[16], Christopher T. Russell[16], Robert Ergun[8], Roy Torbert[4,11], James Burch[11]

1 NASA Goddard Space Flight Center, Greenbelt, MD, USA
2 Boston University, Boston, MA, USA
3 University of Maryland, College Park, MD, USA
4 University of New Hampshire, Durham, NH, USA
5 Swedish Institute of Space Physics, Uppsala, Sweden
6 CNRS/Ecole Polytechnique/Sorbonne Université/Univ. Paris Sud/Observatoire de Paris, Paris, France
7 Imperial College London, London, UK
8 Laboratory for Atmospheric and Space Physics, University of Colorado Boulder, Boulder, CO, USA
9 Denali Scientific, Healy, Alaska, USA
10 Dartmouth College, Hanover, NH
11 Southwest Research Institute, San Antonio, TX, USA
12 Los Alamos National Laboratory, Los Alamos, NM, USA
13 University of Texas at Arlington, Arlington, TX, USA
14 The Aerospace Corporation, El Segundo, CA, USA
15 The Johns Hopkins University Applied Physics Laboratory, Laurel, MD, USA
16 University of California, Los Angeles, Los Angeles, CA, USA

Abstract:
In this paper, we report Magnetospheric Multiscale (MMS) observations of the dayside magnetosphere when the upstream Alfvén speed rises above the solar wind speed (sub-Alfvénic), causing the windsock-like magnetosphere to transform into Alfvén wings. The event occurred in the magnetic cloud of a Coronal Mass Ejection (CME) on April 24, 2023. We highlight the following outstanding features: (1) a layer of accelerated cold CME flow directly adjacent to the wing and to the magnetopause, which presents a rare regime of magnetopause interaction with unshocked CME plasma; (2) moving filaments of the Alfvén wing created by reconnection, which represent new channels of magnetic connection between Earth's magnetosphere and the foot points of the Sun's erupted flux rope; (3) cold CME ion deceleration with little heating across the magnetopause. The reported MMS measurements advance our knowledge of CME interaction with planetary magnetospheres, and open new opportunities to further understand how sub-Alfvénic plasma flows impact astrophysical bodies such as Mercury, moons of Jupiter, and exoplanets that are close to their host stars.

Introduction

An erupted magnetic flux rope from the Sun in the form of fast Coronal Mass Ejection (CME) arrives at the Earth on April 24, 2023. Within the flux rope is a lower density plasma parcel that brings the local Alfvén speed to above the solar wind speed for two hours. The Earth's magnetosphere has been shown to transform into Alfvén wings during long duration (> 1 hour) sub-Alfvénic solar wind by MHD simulations [Ridley, 2007; Chané et al., 2015; Chen et al., 2024; Burkholder et al., 2024].

To date, observations of the magnetosphere's interaction with long-duration sub-Alfvénic solar wind have only been reported in three prior papers. Geotail observations at GSE [X, Y, Z] ~ [-11: -20, 28: 23, 5] R_E by Chané et al. [2012] captured the dusk Alfvén wing and an adjacent layer of flows faster than the concurrent solar wind. The authors termed the enhanced flow layer the outer Alfvén wing, as it is immediately outside of the reduced flow region of the (inner) Alfvén wing. The plasma properties (e.g., density, temperature, and energy distribution) of the enhanced flow layer are not known. The observations by Lugaz et al. [2016] focus primarily on the inner magnetosphere, in particular the radiation belt electron loss, and observed neither the enhanced flow layer nor the Alfvén wings. The work by Hajra and Tsurutani [2022] shows statistics of the sub-Alfvénic solar wind properties and associated changes in the outer radiation belt electron fluxes as well as the geomagnetic SYM-H and auroral ionospheric SML indices, and does not address the Alfvén wings. In this paper, we report dayside measurements of (1) plasmas in the enhanced flow layer to distinguish it as a layer with accelerated and unshocked cold CME solar wind directly against the Alfvén-wing magnetosphere, (2) filaments of hot plasmas, identified as newly reconnected flux tubes added to either the Alfvén wings or the closed field lines of the magnetosphere, and (3) complete transition from the accelerated CME solar wind into the closed field line region of the magnetosphere to show cold CME ion deceleration with little heating. The measurements are from the Magnetospheric Multiscale (MMS) mission [Burch et al., 2016]. This event is the only time a long duration sub-Alfvénic solar wind occurs in the mission life of MMS so far. With its unprecedented high-cadence three-dimensional plasma measurements, MMS records a rare regime of magnetopause reconnection in which channels of magnetic connection between the Sun's erupted flux rope and Earth's magnetic fields are created.

For sub-Alfvenic solar wind with a dominant dawn-dusk (y) IMF, global MHD simulations [Chané et al., 2015; Burkholder et al., 2024; Chen et al., 2024] demonstrate the formation of dawn-dusk wings. In the April 2023 CME magnetic cloud, MMS approaches the edge of the southern dawn wing on the dayside at GSE [10.7, -7.9, -6.8] R_E.

Observations

For the presented MMS data, the magnetic fields are measured by the Flux Gate Magnetometer [Russell et al., 2016], thermal plasma Fast Plasma Investigation [Pollock et al., 2016], and nonthermal particles Fly's Eye Energetic Particles spectrometers [Blake et al., 2016].

Vectors are shown in the Geocentric solar ecliptic coordinate system.

We begin with an overview of the CME observed by MMS2 and Wind in relation to the geomagnetic storm development (Figure 1). The fast-moving CME created an interplanetary (IP) shock and a sheath region in front of the expanding flux rope, the magnetic cloud. Arrival of the IP shock and the southward IMF in the CME sheath initiate the main phase of a geomagnetic storm. The storm development stalls as the IMF B_z turns from southward to northward in the CME sheath and stays mostly northward until entry into the magnetic cloud where B_z is strongly southward (Figures 1b and 1g). In the magnetic cloud, IMF B_z slowly rotates from strongly southward to northward. The CME sheath (bounded by the cyan and magenta vertical lines) is prominently marked by (1) enhanced fluxes of 60-560 keV electrons and ions with the strongest fluxes and highest energy reached at the IP shock arrival (Figures 1c-1d), and (2) the IMF southward turning (Figure 1b) and density drop (Figure 1e). The accelerated particles at the IP shock attain energies even higher than those in the shown inner-magnetosphere interval (~17 UT on 2023-04-24). In the magnetic cloud, MMS encountered Earth's bow shock multiple times. MMS registers a double-peak density pulse at the second bow shock crossing (Figure 1e), coincident with a spike in M_A (Figure 1f) and a bipolar pulse in SYM-H (Figure 1g). This bow shock crossing has been analyzed in depth [Graham et al., 2023]. The density pulse consists of three ion species (a subject of forthcoming papers), and results in extreme responses of the geomagnetic field [Zou et al., 2024].

MMS monitors the magnetosheath interaction with the magnetic cloud (MC) continuously after its last bow shock crossing at ~4:20 UT (Figures 1b, 1e), and particularly as the solar wind Alfvén Mach number $M_A = V_{sw}/V_A$ (where V_{sw} is the solar wind speed and V_A is the Alfvén speed in the solar wind) drops and rises back and forth culminating in the two-hour interval (~12:30-14:30 UT) when M_A stays at ~0.6 (Figure 1f). Before this interval, M_A drops below 2 upon exit out of the CME sheath and entry into the magnetic cloud (Figure 1f). The sub-Alfvénic solar wind is caused by the low density and high IMF strength rather than a decrease in V_{sw} (Figures 1e and 1h) in the strong magnetic field of the MC. The interval is concurrent with a SYM-H plateau at ~ -120 nT (Figure 1g), indicating that the ring current intensity is being held at a level stronger than that of most geomagnetic storms. We show the Wind magnetic field measurements (Figure 1a; without any time shift to preserve its original variations in time) to enable discernment of magnetic variations from the CME magnetic cloud and those due to interaction with Earth's magnetosphere. At ~14:30 UT, MMS observes the closed-field-line region of the magnetosphere with the magnetic field components similar to those observed in the magnetosphere (at the end of the shown interval).

MMS observes the Earth's magnetosheath plasma evolving from shocked (decelerated and heated; marked by the first magenta bar in Figure 2) to unshocked solar wind (beginning is marked with a blue arrow) just before 13 UT, and back to the unshocked solar wind after ~1440 UT (second magenta bar). During the interval when $M_A<1$, the bow shock becomes weaker, farther away, and eventually disappears [Ripley et al. 2007]. Characteristics of the unshocked solar wind include well-defined narrow energy bands of the cold proton and alpha particles (Figure 2c) at energies consistent with upstream measurements such as those from THEMIS B (Figure 2h). The unshocked solar wind flow become faster and faster (Figure 2b) due to local acceleration. The maximum flow speed before entry into the Alfvén wing filaments is ~700 km/s

and is ~800 km/s at exit (14:38 UT), faster than the concurrent solar wind speed (V_{sw}~550 km/s dominated by V_x~ -500 km/s). A analogous layer of enhanced flows was reported based on Geotail measurements at the nightside northern dusk flank at GSE [X, Y, Z] ~ [-11: -20, 28: 23, 5] R_E, and termed the outer wing (Chané et al., 2012). Here MMS explores the dayside base of the southern dawn wing at GSE [10.7, -7.9, -6.8] R_E, with access to open field lines connected to the dawn wing and closed field lines, distinct from the Geotail observation region which allows access only to the dusk-wing open field lines. MMS measures the plasma in the layer of enhanced flow to be cold and unthermalized low-beta wind within the CME flux rope (further information in Figures 3-5). Note that this layer of cold and accelerated CME plasma is now the immediate upstream of the wings and magnetopause.

As a contrast to the enhanced flows at the MMS location, THEMIS B in the solar wind on the dayside (at GSE [34.6, 48.5, 4.5] R_E at 14 UT) orbiting the Moon does not observe the increasing flow, rather, V~V_{ix} ~ -500 km/s from 1330 to 16 UT (Figure 2g). The solar wind flow from OMNI (Figure 1h; observed at L1 and propagated to the model bow shock nose) does not show the increase observed by MMS (Figure 2b), either. The concurrent solar wind speed (from OMNI) is ~550 km/s, substantially lower than the maximum ion flow speed observed by MMS just before encountering the flux tubes (at ~ 14:05 UT) of the dawn wing and the magnetosphere. The correlated discontinuities in THEMIS B magnetic field (Figure 2f) and ion energy distribution (2h) correspond to the bow shock crossing the spacecraft (right before and after 10UT, just after 11 UT, and after 16 UT), indicating that the bow shock expands to the Moon distance as M_A approaches 1 from above.

At ~14:30 UT when V_i~0, the density and magnetic field components resemble those in the magnetosphere (at the very end of the interval in Figure 2). The strongly positive B_z and B_x (> ~20 nT) are consistent with the fact that MMS enters the magnetosphere from the southern hemisphere just outside (equatorward) of the cusp (if the entry into the magnetosphere is inside the southern cusp, B_z would be negative). The weak negative B_y is consistent with the pre-noon location of MMS. However, the energy distributions of ions and electrons show negligible flux of ions below 100 eV, ion flux above ~3 keV is weaker than that in the magnetosphere at 16:30 UT, and electron flux enhancement only at energies below 5 keV - distinct from those at 16:30 UT. The plasma properties suggest that the closed field line region is a fresh closed field line region formed during the storm, and possibly during the sub-Alfvénic interval based on estimates of the time needed for newly reconnected flux in the nightside to convect to the dayside (~30 minutes based on global MHD simulation results in [Chen et al., 2024]) where MMS is.

In the interval shown in Figure 3, MMS begins to encounter magnetic flux tubes that contain electrons and ions that are distinctly more energetic than the unshocked CME MC plasma (Figures 3c and 3e). The ions with energies 20 keV and above are observed, while the CME MC protons are at ~3 keV and alpha particles at ~6 keV (Figure 3c). The energy flux of the energized electrons peaks at 200-1000 eV, in contrast to the CME MC electron flux maximizing below 200 eV at ~14:07 UT (Figure 3e). The isolated flux tubes (sandwiched by MC intervals) correspond to excursions in the magnetic field (Figure 3a) and ion velocity (Figure 3b), energized or thermalized MC ions (Figure 3c), and density spikes (Figure 3d). We name these isolated flux tubes (14:05-14:24 and 14:37-14:38 UT) filaments. The filaments contain field lines with at least one end connected to the Earth, an interpretation based on the assumption that the energized

electrons and ions are either of Earth origin or due to interaction between the MC and the magnetosphere such as reconnection. This assumption is justified by the fact that no significant ion flux enhancements above 5 keV are observed by THEMIS B in the near-Earth upstream. Prior to the shown interval, MMS registers the MC plasma and field lines which have both ends at the Sun.

The 2-hour long sub-Alfvénic interval is concluded with a sudden density rise at ~14:39 UT. This density rise is inherent in the CME MC, as it is observed by Wind and THEMIS B spacecraft (not shown). Upon exit from the magnetosphere and back into the unshocked solar wind, MMS detects the CME MC proton energy at 3-4 keV, corresponding to velocities 750-850 km/s (enhanced flow layer in Figure 2b), and then drops to 1-2 keV at ~14:38 UT (Figure 3c), concurrent with the sudden density increase (Figures 3c-d), signaling the end of the sub-Alfvénic interval locally at MMS. After the density rise, ions regain their "shocked" appearance (the second magenta bar between Figures 2b and 2c).

From 14:25 to 14:35 UT, MMS probes a primarily closed field line region that appears to be freshly generated during the storm. Enhanced fluxes of 60-150 keV electrons (Figure 3f) at pitch angles approximately 90 degrees (Figure 3g) are interpreted as the closed field line regions based on the following: (1) the pitch angle distribution peaks at approximately 90 degrees, consistent with electrons being trapped. (2) Examination of parallel and perpendicular temperatures of lower energy (0.01-20keV) electrons rules out that the energetic electron flux peaking at 90 degrees is due to perpendicular heating (data not shown; full characterization of the electron distribution functions is forthcoming in a separate study). (3) Ion flows are stagnant or weak, and ions and electrons are hot, consistent with the expected magnetosphere condition. (4) The magnetic field is roughly consistent with expected Earth's magnetic field with $B_z>0$, $B_x>0$ (MMS at Z_{GSE} ~ -6.8 RE), and $B_y<0$ at the MMS location. (5) The density (0.25 cm^{-3}) is consistent with magnetospheric density, and lower than the CME MC plasma density (0.5 cm^{-3}).

The regions without trapped energetic electrons could contain open (one end connected to the Earth and the other to the Sun's corona) or recently closed (but not yet populated with ~100 keV energetic electrons) field lines. The parallel and anti-parallel thermal electron fluxes in Figure 4 further support that at least a subset of these regions consists of both open and closed field lines, as will be discussed below.

We zoom in the entry into and exit out of the magnetosphere to highlight the dawn wing filaments and ion mixing/deceleration/heating (Figure 4). We interpret filaments/regions with no discernable field-aligned anisotropy as closed field lines (such as that at the end of the interval in Figures 4a1-f1). At entry into the primarily closed field line region, MMS encounters regions with electrons energized to above 100 eV and much stronger flux parallel to B (marked by cyan bars and shaded in Figures 4a1-f1), consistent with filaments of the dawn wing generated by reconnection in the southern hemisphere. These regions tend to have hot ions, and less discernable cold MC ions. The parallel electrons above 2 keV are interpreted as energized by southern cusp reconnection (such as that depicted by the southern-cusp red arrow in Figure 5h). The ions in the interval 14:23:20-14:23:23UT maintain their MC-like cold temperature, and both parallel and anti-parallel electrons below 200 eV exhibit MC-like energy distribution in addition to the keV parallel electrons, showing mixing of MC plasma with reconnection-energized

plasma. Note that based on examination of the global MHD simulations [Chen et al., 2024], the most probable southern cusp reconnection locations are primarily on the duskside of the Earth, and of order 10 R_E away from MMS. For reference, electrons at 1 keV travel this distance in 1.8 s.

At exit back into the unshocked solar wind, electrons at ~1 keV moving anti-parallel to the magnetic field are observed (marked by magenta bars and shaded in Figure 4a2-f2) prominently, providing evidence for MC IMF field lines that have just been newly reconnected at locations north of MMS. These magenta intervals show MC-like ions (Figure 4a2) with the anti-parallel electron flux (Figure 4c2) dominating over the parallel flux (Figure 4b2) in the energy range 200-2000 eV. Note that the parallel flux exhibits an energy distribution similar to the ambient MC electron energy distribution (such as that at ~14:38:15UT). The corresponding ion reduced distributions in v_{ixyz} (Figures 4d2-f2) further consolidate that the ion velocity distributions are approximately the ambient MC v_{ixyz} distributions shown at ~14:38:15 UT, for example.

The ion v_{ixyz} distributions reveal ion deceleration, thermalization, and mixing under the unusual condition of the cold unshocked solar wind directly coming against the magnetopause (boundary between closed field lines of the magnetosphere and the IMF) and the Alfvén wing (open field lines with one end at Earth). Cold MC ions penetrate into the closed field line region, such as those in the intervals centered at ~14:23:26, 14:23:40, 14:23:55, 14:24:22 UT (Figures 4d1-f1), and at 14:36:05 and 14:37:15 UT (Figures 4d2-f2). Some of the cold MC ions are decelerated to $v_{ix} \sim 0$ (~14:23:40UT), and their distribution in v_{iy} is altered from peaking at -300km/s to 100km/s, while keeping v_{iz} approximately the same as the ambient MC $v_{iz} \sim$ -300km/s. Ions observed in the interval between 14:36:15-14:36:27 UT are largely thermalized with no discernable cold solar wind-like populations, and the distribution is relatively symmetric with respect to $v_{ix} = 0$, while biased toward positive v_{iz} and negative v_{iy}, indicating a northward and dawnward flow on closed field lines (field line topology inferred from the roughly equal parallel and anti-parallel electron flux). Apart from this interval, MMS observes clear trace of the cold solar wind ion population as it exits back to the unshocked solar wind, even when the population has been decelerated. One such example is the distribution at ~14:36:00UT (Figures 4d2-f2) when the phase space density peak (narrow red band) is at $v_{iy} \sim 0$, and slightly negative v_{ix}, substantially slower than the ambient MC flow.

We zoom in example filaments to show structures and dynamics of the ions and electrons (Figure 5). The cold proton population is at ~2 keV. The filaments exhibit magnetic field (Figure 5a) and ion flow (Figure 5g) excursions, energized ions (Figure 5b), flux enhancements of energized keV electrons parallel (Figure 5c) and anti-parallel (Figure 5d) to B, electron density spikes and depressions within (Figure 5e). The ion phase space density shows distinct distributions in v_{ix}: the filaments at 14:08:05 and 14:08:10 UT are substantially colder than the ones after 14:08:20 UT. The filaments are not due to MMS entering into and coming out of the magnetosphere, based on the associated V_{ixyz} (Figure 5g) and B_{xyz} (Figure 5a). Rather, their y-component velocities (V_{iy}) tend to be stronger than the ambient MC flow along -y (suchas that at 14:08:20 UT), indicating strong dawnward motion that is consistent with reconnected flux tubes moving toward dawn.

We interpret the filaments with energized colder ions before 14:08:20 UT as encounters with flux tubes that have just been produced by reconnection. Only energized ions are observed in the 'new-born' (newly reconnected) flux bundles. If reconnection occurs farther away from MMS, lower energy ions can have access to the spacecraft. We therefore interpret the structures with ions below the solar wind energy (after 14:08:20 UT) as flux tubes that have reconnected farther back in time (and spatially farther away from MMS) than those before 14:08:20 UT. Both types of filaments contain open field lines (shaded intervals) from the southern hemisphere as part of the dawn wing.

As illustrated in Figure 5h based on data from a global MHD simulation [Chen et al., 2024], two types of Earth-connected field lines at the MMS location are the most likely: (a) dawn wing - southern hemisphere field lines connected to the IMF in the CME flux rope, and (b) closed field lines connected to the southern and northern hemispheres. These magnetic field lines are traced from the surface of $r = 3R_E$ from uniformly distributed seed points covering the entire 3D sphere, and hence representative of all possible field line topologies within the simulation. The closed field lines are in green, and open field lines coming out of (going into) the southern (northern) hemisphere in red (blue). The open field lines extending towards dawn at $Y<0$ and dusk at $Y>0$ form two wings connecting the Earth and the Sun magnetically.

To produce dawn-wing filaments that can cross the trajectory of MMS, reconnection can occur (1) in the southern hemisphere, yielding energized electrons parallel to the magnetic field at the MMS location (Figure 5h "newly reconnected" red field line and the red arrow on green field line are simulation examples; blue shaded intervals in Figures 4b1-c1 are MMS examples); (2) in the northern hemisphere, giving rise to energized electrons anti-parallel to **B** (red arrow as one example reconnection site for the "to be reconnected" green field line in Figure 5h; magenta shaded intervals in Figures 4b2-c2). MMS is less likely to observe the dusk wing field lines (from the Sun and into Earth's northern hemisphere), because they are produced by reconnection between the MC field lines and closed magnetosphere field lines duskward of MMS in the southern hemisphere and northward of MMS in the northern hemisphere (blue "newly reconnected" field line in the southern hemisphere and the three white field lines in the northern hemisphere are examples). Upon reconnection, new dusk wing field lines convect duskward and unlikely cross the path of MMS in the dayside southern dawn sector.

We leave it an open possibility to have MMS observe a dusk wing filament. During storm time, field line connectivity can be so wild as to have a southern-dusk field line going into the northern hemisphere on the dawn side, such that upon reconnection, the dayward and duskward convection of the field line will bring it across MMS. The implication is that dusk wing and dawn wing open field lines may meet on the dayside and produce closed field lines. Reconnection scenarios more complicated than the ones illustrated in Figure 5h are possible. In addition to producing closed field lines on the dayside, other examples include: IMF reconnecting with dawn wing field lines in the form of a winding flux rope (such that a component anti-parallel to IMF is present for reconnection), and dawn-wing field lines reconnecting with themselves under flux rope configurations. We leave it for future work to address observable differences for various scenarios.

Summary and Conclusion:

During the April 2023 CME when the solar wind is sub-Alfvénic, MMS observes (1) the magnetosheath evolving from shocked to unshocked CME solar wind, (2) in the magnetic cloud (MC), a layer of accelerated cold solar wind flow adjacent to the dawn wing and the magnetopause, and (3) a transition region from the unshocked and accelerated MC flow in the IMF to the dayside closed field-lines of the magnetosphere with dawn Alfvén wing flux tubes connecting the Earth and the Sun. Cold CME ions with various degree of deceleration penetrate into the closed field line region. In other words, the magnetopause (boundary between IMF and closed field lines of the magnetosphere) is where the MC solar wind plasma gets decelerated and heated, in contrast to the typical super-Alfvénic solar wind condition where the bow shock decelerates and heats the solar plasma several R_E upstream from the magnetopause. What processes decelerate and heat the CME plasma across the magnetopause?

The sub-Alfvénic solar wind interaction with the magnetosphere creates a rare regime of magnetopause reconnection. Cusp reconnection occurs at the boundary between Earth's closed field lines and the MC field lines loaded with CME plasma. Instead of the heated and decelerated solar wind in the form of the usual magnetosheath plasma with a typical plasma beta above 1, now the immediate upstream of the magnetopause is cold and accelerated CME plasma with field lines connected to the foot points of erupted flux rope at the Sun. The beta in this CME flux rope is as low as 0.01, in contrast to the typical magnetosheath beta > 1. Lower beta has been demonstrated to support faster reconnection [Zenitani and Miyoshi, 2020], and stronger production of nonthermal particles [Li et al., 2021]. The magnetopause reconnection with the low beta CME solar wind as its upstream resembles that at the inner planets (such as Mercury) of the solar system and at magnetized exoplanets close to their stars.

What prevents the ring current from being dissipated during the sub-Alfvénic interval is an intriguing question. SYM-H stays approximately constant at -120 nT (ring current stronger than most geomagnetic storms), prolonging the storm recovery. What happens in the magnetosphere to hold the ring current intensity for these two hours? Do injections of energetic ions occur to replenish the ring current at a rate roughly balancing the loss, leading to a roughly constant SYM-H during the interval? If so, how do the injections relate to nightside magnetic reconnection under the Alfvén-wing magnetosphere configuration?

Sun-Earth magnetic connection through Alfvén wings is analogous to the Jupiter-Ganymede connection. In the sub-Alfvénic flow inside the Jovian magnetosphere, Jupiter's moon Ganymede always exhibits the Alfvén-wing magnetosphere configuration [Kivelson et al., 2004; Wang et al., 2018; Zhou et al., 2019]. Recent observations from the Jovian Auroral Distributions Experiment aboard Juno capture enhanced electron fluxes, including accelerated, magnetic field-aligned electrons at Ganymede's magnetopause, and are interpreted as evidence of magnetic reconnection [Ebert et al, 2022]. Auroral emissions at Ganymede (by Juno Ultraviolet Spectrograph) during the same flyby support that the precipitating electrons are accelerated by magnetic reconnection [Ebert et al, 2022]. Here at Earth, MMS measurements of the dawn wing filaments indicate that newly reconnected flux bundles become part of the wings, a dynamic process to continuously replenish the wing. MMS observations of this MC-magnetosphere interaction teach us that the Ganymede aurora is likely powered by magnetic reconnection, and

that the Earth loses its plasma to the solar corona through the wings. Conversely, solar electrons from the foot points of the Sun's erupted flux rope may be accelerated and precipitate into Earth's ionosphere to form Alfvén wing aurora – a possibility to be checked out by future work.

Open Research

MMS data are publicly available at https://lasp.colorado.edu/mms/sdc/public/. Wind and THEMIS B data are obtained from the CDAWeb https://cdaweb.gsfc.nasa.gov/index.html/. The SWMF model, including BATS-R-US and the ionosphere model, is publicly available through GitHub (https://github.com/SWMFsoftware). The simulation input and output files are posted at the Zenodo repository (https://doi.org/10.5281/zenodo.10445643).

Acknowledgments

This work is supported by the NASA MMS Mission.

References:

Burch, J. L., Torbert, R. B., Phan, T. D., Chen, L. J., Moore, T. E., Ergun, R. E., et al. (2016). Electron-scale measurements of magnetic reconnection in space. Science, 12, aaf2939. https://doi.org/10.1126/science.aaf2939

Burkholder, B. L., L.-J. Chen, M. Sarantos, D. J. Gershman, M. R. Argall, Y. Chen, C. Dong, F. D. Wilder, O. Le Contel, H. Gurram (2024), Magnetic Reconnection During Sustained sub-Alfvénic Solar Wind Driving, GRL, under review

Blake, J. B., Barry Mauk, et al. (2016). The Fly's Eye Energetic Particle Spectrometer (FEEPS) Sensors for the Magnetospheric Multiscale (MMS) Mission, Space Sci Rev 199, 309–329 (2016). https://doi.org/10.1007/s11214-015-0163-x

Chané, E., Saur, J., Neubauer, F., Raeder, J., & Poedts, S. (2012). Observational evidence of Alfvén wings at the Earth. Journal of Geophysical Research: Space Physics, 117 (A9).

Chané, E., Raeder, J., Saur, J., Neubauer, F., Maynard, K., & Poedts, S. (2015). Simulations of the earth's magnetosphere embedded in sub-Alfvénic solar wind on 24 and 25 May 2002. Journal of Geophysical Research: Space Physics, 120 (10), 8517–8528.

Chen, Yuxi, Chuanfei Dong, Li-Jen Chen, Menelaos Sarantos, Brandon Burkholder (2024), Interplanetary magnetic field By controlled Alfvén wings at Earth during encounter of a coronal mass ejection, arXiv:2402.04282

Graham, D. B., Yu. V. Khotyaintsev, A. P. Dimmock, A. Lalti, J. J. Boldu, S. F. Tigik, S. A. Fuselier (2023). Ion Dynamics Across a Low Mach Number Bow Shock, arXiv:2311.11373

Li, X., et al. (2017), Particle Acceleration during Magnetic Reconnection in a Low-beta Plasma, 2017 ApJ 843, 21, DOI 10.3847/1538-4357/aa745e

Lugaz, N., Farrugia, C. J., Huang, C.-L., Winslow, R. M., Spence, H. E., and Schwadron, N. A. (2016). Earth's magnetosphere and outer radiation belt under sub-Alfvénic solar wind. Nature Communications, 7, 13001.

Kivelson, M., Fran Bagenal, William Kurth, Fritz Neubauer, Chris Paranicas, Joachim Saur (2004), Magnetospheric Interactions with Satellites, In: Jupiter. The planet, satellites and magnetosphere. Edited by Fran Bagenal, Timothy E. Dowling, William B. McKinnon.

Pollock, C., Moore, T., Jacques, A., Burch, J., Gliese, U., Saito, Y., et al. (2016). Fast Plasma Investigation for Magnetospheric Multiscale. Space Sci.
Rev., 199, 331-406. doi: 10.1007/s11214-016-0245-4

Ridley, A. J. (2007). Alfvén wings at earth's magnetosphere under strong interplanetary magnetic fields. Annales Geophysicae, 25 (2), 533–542.

Russell, C. T., Anderson, B. J., Baumjohann, W., Bromund, K. R., Dearborn, D.,
Fischer, et al. (2016). The magnetospheric multiscale magnetometers.
Space Sci. Rev., 199 , 189-256. doi: 10.1007/s11214-014-0057-3

Wang, L., et al. (2018), Electron Physics in 3-D Two-Fluid 10-Moment Modeling of Ganymede's Magnetosphere, JGR - Space Physics
(2018) https://agupubs.onlinelibrary.wiley.com/doi/10.1002/2017JA024761

Ebert, R. W., et al. (2022), Evidence for Magnetic Reconnection at Ganymede's Upstream Magnetopause During the PJ34 Juno Flyby, Geophysical Research Letters
(2022). https://agupubs.onlinelibrary.wiley.com/doi/full/10.1029/2022GL099775

Zenitani, Seiji, and Takahiro Miyoshi (2020). Plasmoid-dominated Turbulent Reconnection in a Low-β Plasma, The Astrophysical Journal Letters, 894:L7

Zhou, H., Toth, G., Jia, X., Chen, Y., and Markidis, S. (2019). Embedded kinetic simulation of Ganymede's magnetosphere: Improvements and inferences. Journal of Geophysical Research: Space Physics, 124 (7), 5441–5460.

Zou, Y., J. W. Gjerloev, S. Ohtani, M. Friel, J. Liang; L. R. Lyons; Y. Shen, J. Liu, L.-J. Chen, B. Ferdousi, A. Chartier, S. Vines, & C. L. Waters (2023), An Extreme Auroral Electrojet Spike during 2023 April 24th Storm, under review in AGU Advances

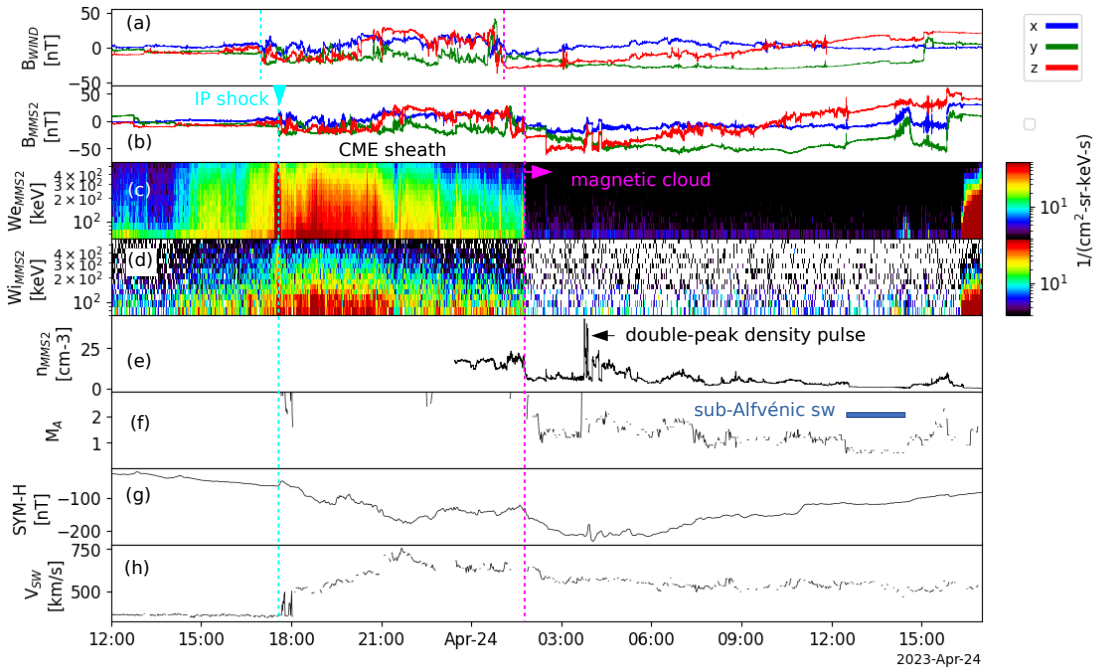

Figure 1. Overview of the 2023 April CME and the geomagnetic storm triggered by it. (a) Three components of the magnetic field observed by the Wind spacecraft at L1, and (b) by MMS2 on the dayside, respectively. (c-d) MMS suprathermal electron and ion (60-550 keV) energy fluxes exhibiting strong enhancements at the interplanetary shock and its downstream CME sheath. (e) MMS electron density. (f) The Alfvén Mach number M_A (ratio of the solar wind speed and the Alfvén speed; taken from the OMNI data which has been propagated to the model bow shock nose) drops below 2 upon entry into the magnetic cloud (CME flux rope) where the energetic particle flux enhancements cease. The two-hour interval when M_A <1 is the primary focus of this paper. (g) The geomagnetic storm index SYM-H. (h) The solar wind speed from OMNI.

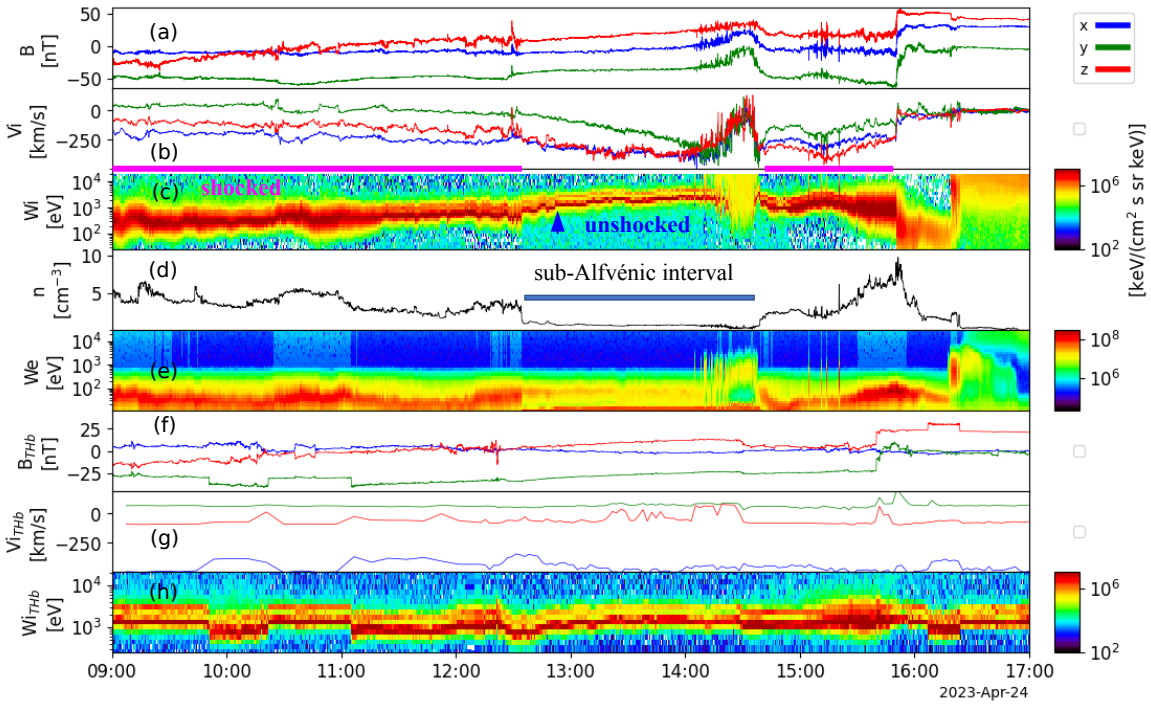

Figure 2. MMS observation of the magnetosheath evolution, Alfvén wing filaments, and magnetosphere to highlight the interaction with the sub-Alfvénic solar wind. (a) Magnetic field components. (b) Ion velocity components. (c) Ion energy flux. (d) Electron density. (e) Electron energy flux. (f-h) Magnetic field components, ion velocity components, and energy flux from THEMIS B (orbiting the Moon at GSE [34.6, 48.5, 4.5] R_E at 14 UT) to provide a near-Earth upstream context for the MMS observation.

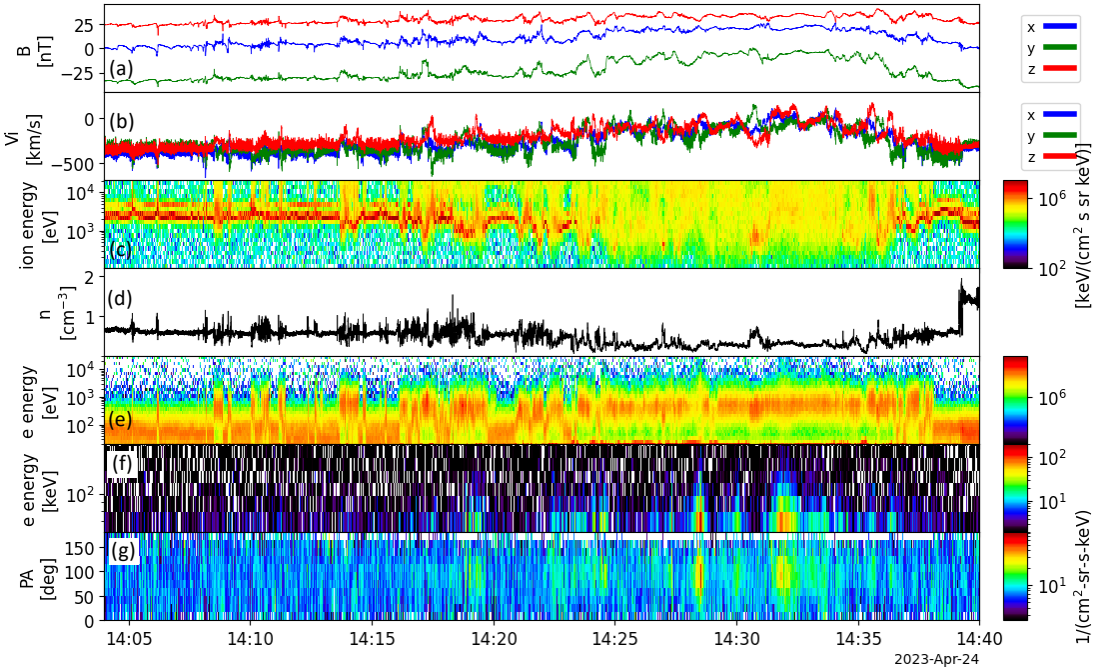

Figure 3. Filaments of the dawn Alfven wing and closed-field-line regions observed by MMS2. (a) Magnetic field components. (b) Ion flow vector. (c) Energy flux of ions (0.2-20 keV). (d) Plasma density. (e) Energy flux of electrons (0.02-3 keV). (f-g) Energetic electron flux (60-200 keV) and their pitch angle (PA) distribution. The intervals with energetic electron flux peaking at pitch angles around 90 degrees are interpreted as closed-field-line regions of the magnetosphere.

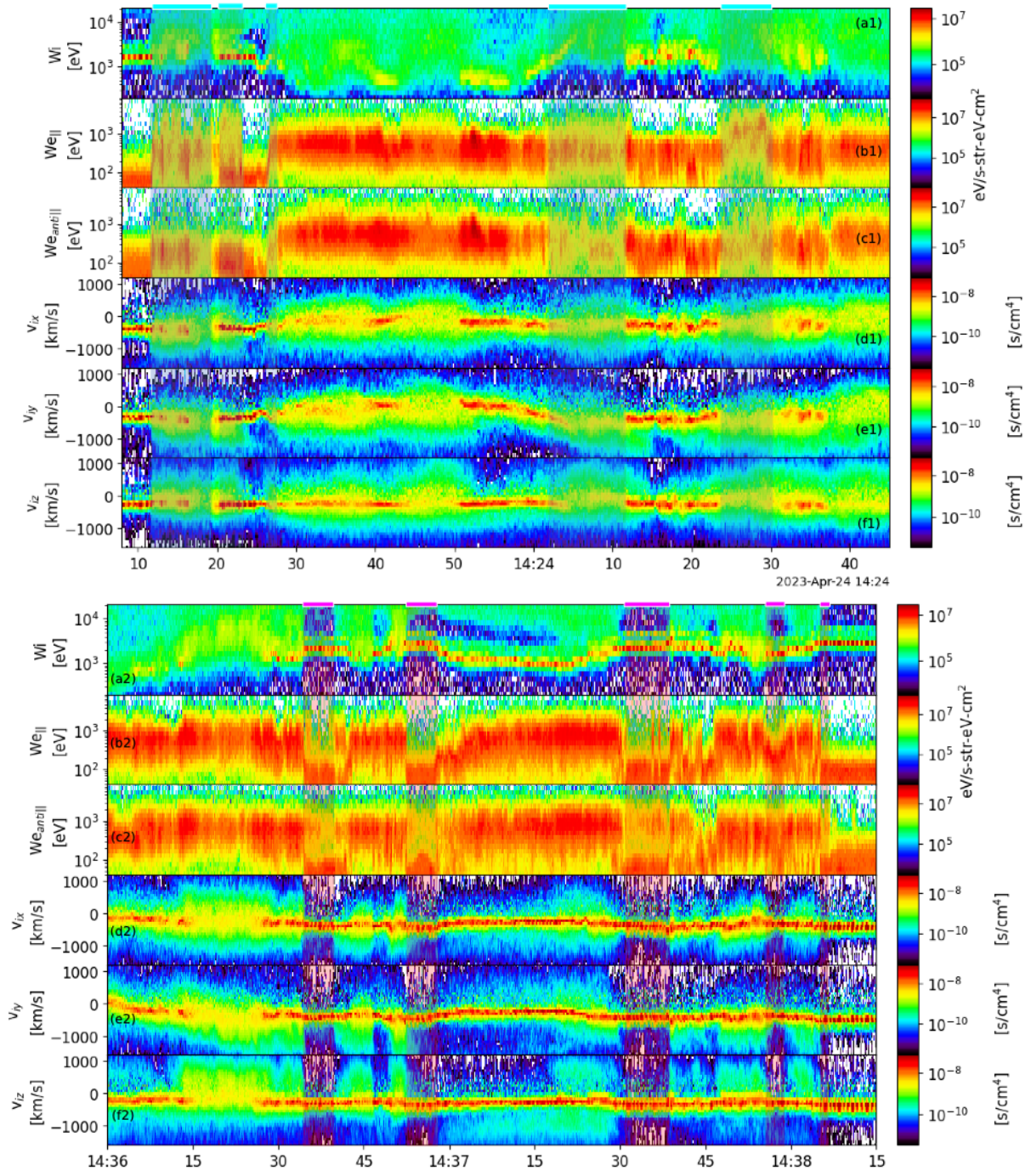

Figure 4. Evidence for the southern/dawn wing flux tubes and cold MC ion deceleration. Entry (a1-f1) into and exit (a2-f2) from the closed field line region of the magnetosphere. (a1,a2) ion energy flux to provide a context for distinct regions based on the cold MC and the hot ions. (b1,b2) electron energy flux parallel to the magnetic field. (c1,c2) electron energy flux anti-parallel to the magnetic field. Ion phase space density (summed over the other two velocity dimensions) as a function of v_{ix} (d1,d2), v_{iy} (e1,e2), and v_{iz} (f1,f2). The cyan (magenta) bars and the shades below them mark the intervals with dominant parallel (anti-parallel) electron fluxes in the 200-2000 eV energy range.

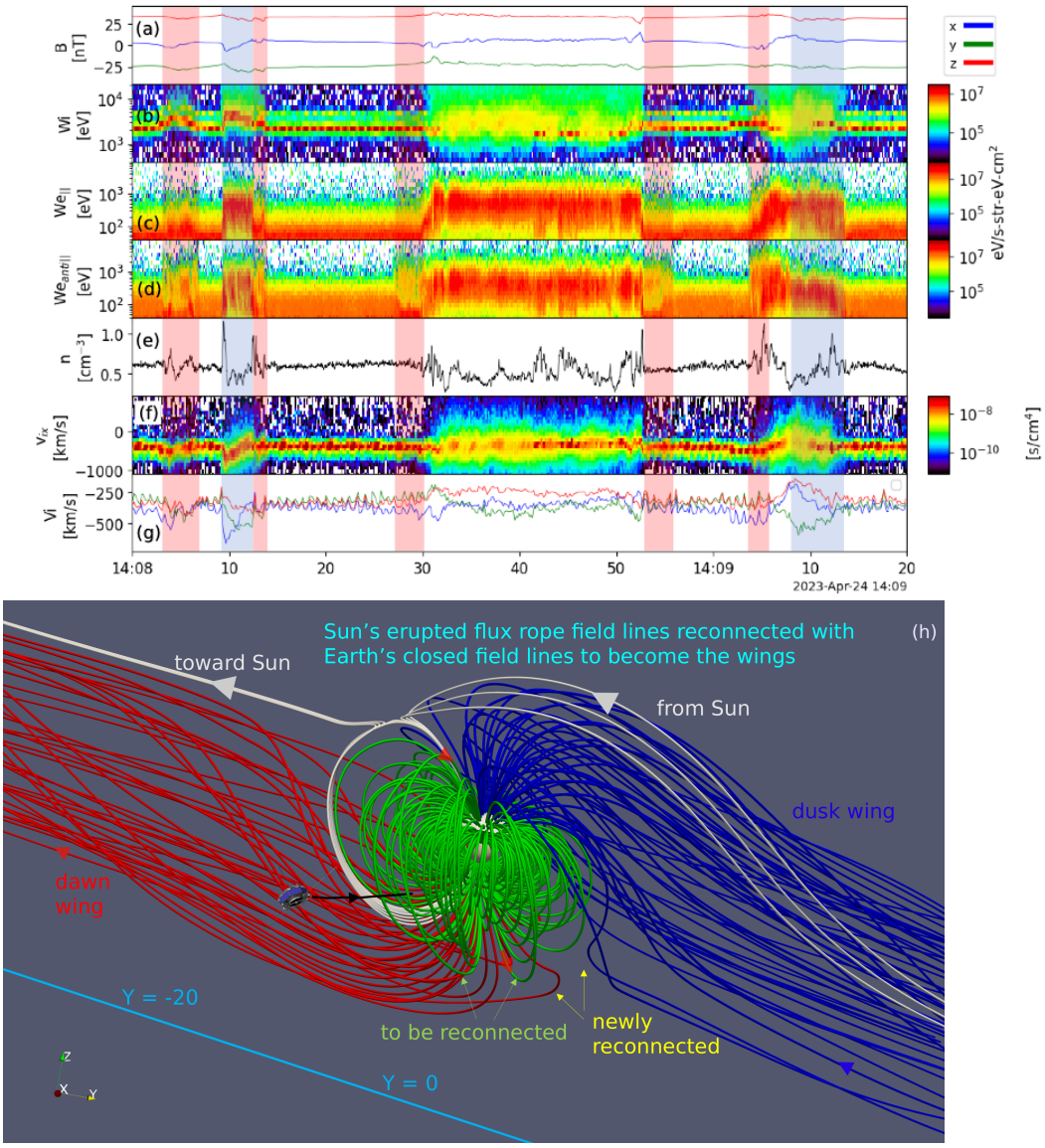

Figure 5. Zoom-in view of example filaments observed by MMS showing distinct plasma dynamics and field line connectivity, and a global field-line illustration. (a) Magnetic field components. (b) Energy flux of ions (0.4-20 keV) summed over all directions. (c-d) Energy flux of electrons (0.02-30 keV) parallel and antiparallel to the magnetic field. (e) Electron density. (f) Ion phase space density (summed over v_y and v_z) as a function of the x-component of the velocity. (g) Ion flow vector. (h) Illustration of the CME flux rope field lines interacting with the Alfvén-wing magnetosphere. The southern-dawn wing is shown in red, northern-dusk wing in blue, closed field lines in green, and example newly reconnected as well as soon-to-be-reconnected field lines in white. Red arrows on green field lines show example locations for potential reconnection.